A Method for the Conceptual Design of Hybrid Electric Aircraft

Zamboni, Jacopo; Vos, Roelof; Emeneth, Mathias; Schneegans, Alexande

DOI
10.2514/6.2019-1587

Publication date
2019

Document Version
Accepted author manuscript

Published in
AIAA Scitech 2019 Forum

A Method for the Conceptual Design of Hybrid Electric Aircraft

Jacopo Zamboni * and Roelof Vos †
Delft University of Technology, Delft, The Netherlands, 2600AA

Mathias Emeneth ‡ and Alexander Schneegans §
PACE America Inc., Seattle, WA, 98115

The growing interest into hybrid electric propulsion as a possible solution to reduce in-flight emissions has led to the investigations of many innovative propulsive system architectures that couple higher system efficiency with improved aerodynamic propulsion integration strategies. The paper presents a methodology to model and size generic hybrid electric propulsion system at the conceptual level allowing for a rapid exploration of the vast design space. The generalization of the propulsive system using a basic propulsive power unit object is discussed highlighting the control parameters needed to fully define the propulsive system architecture. Three case studies for a 2035 turbo-prop regional aircraft using parallel, series/parallel and distributed series configurations show that improvements to the fuel and energy consumption are affected by the system morphology, its control strategy and the maturity level assumed for its components. Using conservative estimations for the battery and electric components performances indicate that the best configurations can only provide a fuel reduction of around 5% while weighting 25% more than the reference design. Using more optimistic assumptions leads to a larger feasible design space where the best performing configuration, the series/parallel one, realizes more substantial fuel and energy reductions of 28% and 14% with a 24% higher take-off mass.

Nomenclature

Latin symbols

C_D	=	Drag coefficient [-]
C_L	=	Lift coefficient [-]
D	=	Drag [N]
E	=	Energy [J]
g	=	Acceleration of gravity [m/s^2]
j	=	Electric current area density [A/m^2]
J	=	Advance ratio [-]
k	=	Correction coefficient [-]
m	=	Mass [kg]
M	=	Mach [-]
$\dot{m}$	=	Mass flow [kg/s]
n	=	Number of [-]
P	=	Power [W]
t	=	Time [s]
T	=	Thrust [N]
V	=	Flight speed [m/s]
W	=	Weight [N]

Greek symbols

ϵ	=	Specific energy [Wh/kg]
η	=	Efficiency [%]
Θ	=	Propulsive power share [%]
ρ	=	Air density [kg/m^3]
$\hat{\rho}$	=	Specific power [kW/kg]
σ	=	Specific resistivity [Ωm^2/m]
Υ	=	Power-lapse [-]
ϕ	=	Shaft power ratio [%]
φ	=	Electric power ratio [%]

Subscripts

bat	=	Battery
cb	=	Cable
E	=	Energy
ec	=	Electric component
eg	=	Electric generator
egt	=	Electric generator - gasturbine system
em	=	Electric motor
emg	=	Electric motor generator
fuel	=	Fuel
gt	=	Gas turbine
ov	=	Overall
P	=	Propulsive power

*MSc. Student, Faculty of Aerospace Engineering, Delft University of Technology, Student AIAA member
†Assistant Professor, Faculty of Aerospace Engineering, Delft University of Technology, Senior AIAA member
‡Senior Business Development Manager, PACE America, AIAA Member
§President, PACE America, AIAA Member

s	=	System
seg	=	Mission segment
sh	=	Shaft
th	=	Theoretical
Tot	=	Total

Acronyms

CAS	=	Calibrated Air Speed
DEP	=	Distributed Electric Propulsion
DoH	=	Degree of Hybridization
ESAR	=	Energy Specific Air Range
HEP	=	Hybrid Electric Powertrain
MTOW	=	Maximum Take Off Weight
OEI	=	One Engine Inoperative
PMAD	=	Power Management And Distribution
PPU	=	Propulsion Power Unit
SOC	=	State Of Charge
TSPC	=	Thrust Specific Power Consumption
YEIS	=	Year Entry Into Service

I. Introduction

The growing concern with global emissions as the air-transport sector keeps expanding is the main driver behind aggressive chemical and noise pollution reduction targets as proposed by several world-wide organizations. To achieve decreases of 75% in CO_2-emissions per passenger kilometre, 90% in NO_x emissions and 65% in perceived noise relative to aircraft of the year 2000 as required by the European Flightpath 2050 project, it is believed that even the most optimistic developments of conventional technologies (air-breathing engines, tube-and-wing configurations) would fall short of the target by 10 to 15% [1–3].

The attention has therefore migrated toward more futuristic solutions that would allow a drastic reduction of fuel consumption. One such solution is the integration of electrically driven propulsive devices into novel aircraft configurations that would leverage the characteristics of the electric machines to also improve the aero-propulsive capabilities of the design. However, a fully-electric aircraft for the transport sector is not seen feasible in the foreseeable future as the disadvantageous mass trade-off between chemical and electric energy storages leads to heavy designs that cannot fulfil the original mission [4, 5]. Still, it appears that electrifying only part of the propulsive system could allow for interesting improvements that could be compounded with the advances in conventional technologies.

The main obstacle when designing hybrid propulsion systems has been that the design space (i.e. the possible choices that can be made) is vaster and more complex. To overcome the shortcomings of well-established design methods, power-based approaches for the sizing of generic multi-energy aircraft have been proposed in the past [6, 7]. These methods can handle multi-energy systems where the propulsive devices are not homogeneous in size.

In this report, a method for the design of hybrid electric system using batteries as the electric energy storage is proposed. The main strengths are its flexibility in the definition of the system morphology, the coupling of the results to constraints and mission requirements and the ability to finely control the power-usage at the segment level.

II. Methodology

The proposed method aims to solve the sizing problem by using an outside to inside power-path approach (from propulsive shaft to energy source) driven by segment specific control laws provided directly by the user or as part of the design vector of an optimization routine. The sizing loop is composed of three main computation modules: the constraint analysis, the point mass analysis and the component sizing module as shown in Figure 1. These loops receive the user inputs in the form of an aircraft configuration, top level requirements for the constraints and mission, and optionally the devices performance maps. When these are not supplied, well-established conceptual design methods are used for the computation of the missing information [8].

The constraint analysis allows the computation of the minimum power to weight ratio to satisfy regulations and point performance requirements. Differently from other existing sizing methodology [9], the resulting power loading is not directly split among the thrust-producing powerplants but it is instead used as a starting point for the point mass analysis carried out in the mission analysis module.

Using the input control laws and components efficiencies, the propulsive power at a given point in the mission is propagated throughout the entire propulsion system starting from the propulsive device (propeller, fan) and ending at the energy sources (battery or fuel). The sizing power for each components of the propulsion system is then set to the maximum value reached during the mission and fed to the component sizing module. By using the computed values of the power-paths it is also possible to evaluate the mission energy requirements through time integration of the power at the energy source.

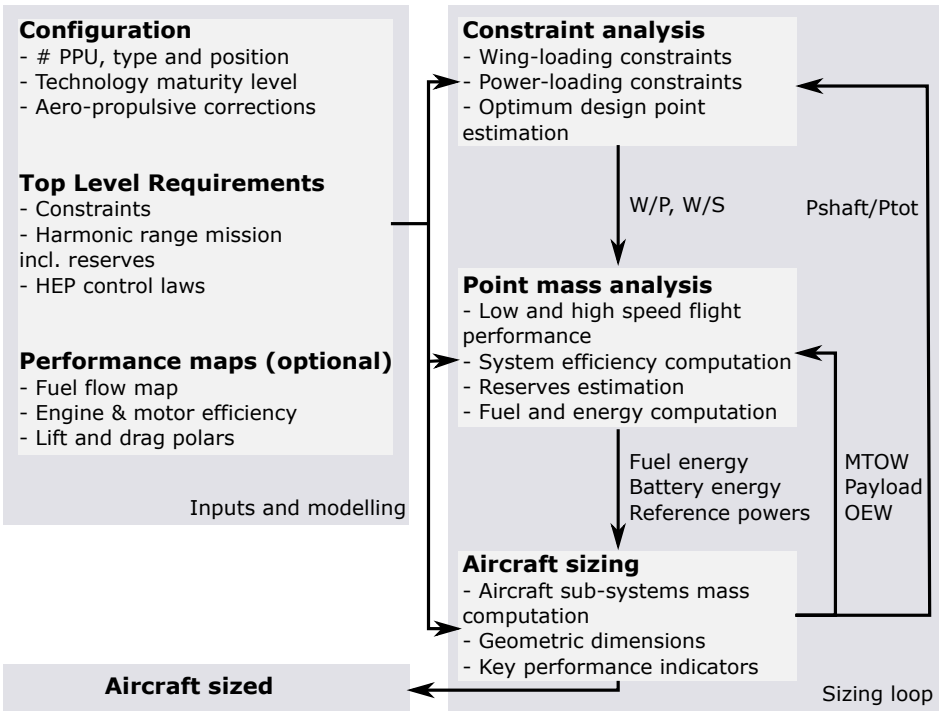

Fig. 1 Flow chart of the proposed methodology for hybrid electric aircraft sizing.

Once the reference powers and energy requirements are known, it is possible to size the aircraft by adding together the masses and dimensions derived from the component specific sizing laws. The sizing module then feeds back these masses to the mission analysis module and the relative shaft power of the propulsive units to the constraint module. The process is then repeated until convergence is achieved and the aircraft is sized. In the following sections, a more in-depth explanation of the first two modules is given. The rules used for deriving the variable efficiencies of each propulsion system component are omitted from this work due to space constraints but can be found in the full report at [10].

A. Hybrid Electric Propulsive Power Unit

To allow the full exploration of the design space made available using a hybrid electric architecture, there is the necessity to define a sub-system object that is complex enough to capture all the possible architecture differences while being simple enough to be usable at the conceptual design phase. The solution proposed in this work is to define each propulsion power unit as a generic object that, depending on three control parameters, can morph into an arbitrarily complex architecture. The naming convention adopted for the overall system follows the work of Thole [4].

Figure 2a shows the generic Propulsion Power Unit sub-system (PPU) highlighting also the division between the side depending exclusively on the single powerplant performance and the side shared by all PPUs. This schema should be read in terms of the power-paths only and not as actual components that exist in each powerplant since, depending on the control parameters, entire branches of components could be absent or shared as shown in Figure 3. The generic propulsive power unit contains energy sources, power distribution and power converter elements.

The energy sources are the chemical energy, contained in the form of fuel in the fuel tank, and electrical energy, stored in the battery packs. The power distributors are all the elements that do not convert energy but either transfer it or split the power along different paths. These are the gearbox, that combines the shaft power of electric motors/generator and conventional gas turbines, and the Power Management and Distribution system (PMAD) that include all the electric components needed such as transformers, inverters, circuit protectors and rectifiers. Finally, the energy converters transform the energy from one form to another. These are the gas-turbine engines, electric motors and generators and propulsive devices. In this study, a propeller is used to convert the shaft power into thrust, but a similar approach could be used for jet-aircrafts using turbo-fans as done in reference [11].

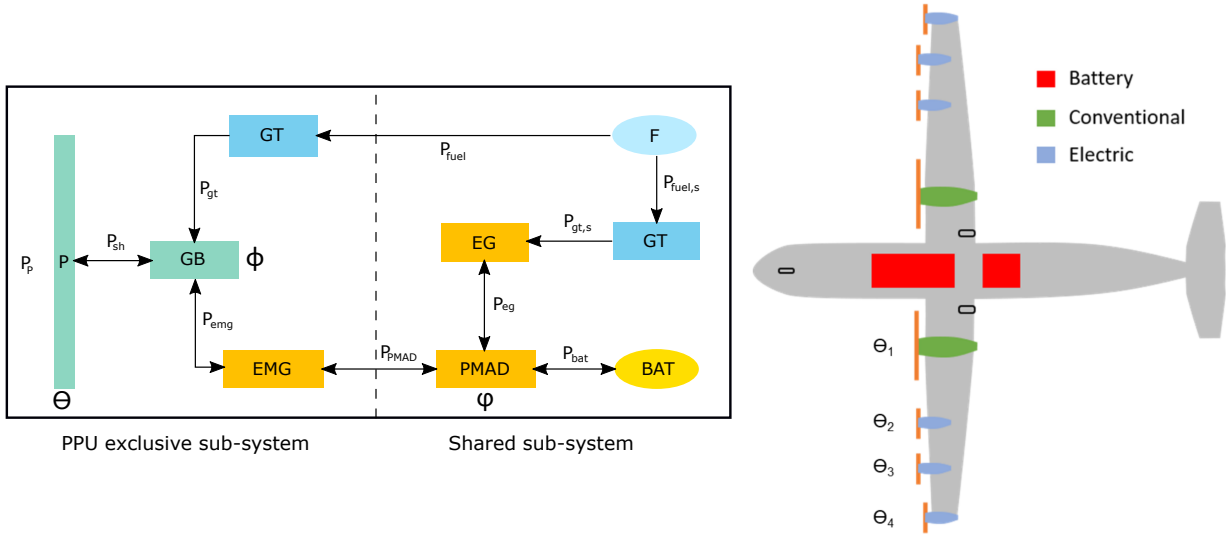

(a) Generic propulsion power unit schema

(b) Propulsion power share over propulsive power units

Fig. 2 Generalization of the propulsion power unit with main control parameters and power-paths

B. Propulsive Power Unit Control Parameters

Two propulsion system parameters and one aircraft-level parameter are used to fully define the power requirements along the possible power-paths. These three parameters are chosen by supplying an appropriate time-dependent control law. Starting at the aircraft level, the *propulsive power share* is defined as the ratio of power supplied by one of the propulsive devices over the total required power as computed from the flight performance module:

$$\Theta_i = \frac{P_{P,\,i}}{P_P} \tag{1}$$

If the propulsive device is connected to an electric motor/generator, Θ_i can be set to negative values changing the propulsive unit from a power user to a power producer thus allowing for in-flight re-charge of the battery packs.

The second control parameter is needed to describe how the power supplied to the gear box is divided between an electric motor and gas turbine mounted in parallel configuration. The *shaft power ratio* is thus defined as the instantaneous shaft power of the electric motor-generator over the total shaft power of the propulsive unit:

$$\phi = \frac{P_{\text{emg}}}{P_{\text{emg}} + P_{\text{gt}}} \tag{2}$$

This parameter can have values in the interval $[0, 1]$ during normal use but it can become negative if the gas turbine is used to produce both propulsive power and re-charge the battery. A constant shaft power ratio of 1 is set for propulsive power units in which the propeller is connected only to an electric motor while $\phi = 0$ is set for conventional powerplants.

A control parameter needs to be used to solve the power-paths of propulsive system that make use of both a battery and a generator as sources of electric power. The *electric power ratio* is defined as the electric power consumed from the battery over the total electric power used by the propulsive unit at a given time:

$$\varphi = \frac{P_{\text{bat}}}{P_{\text{bat}} + P_{\text{eg}}} \tag{3}$$

As for the *shaft power ratio*, this parameter is usually set to a value in the interval $[0, 1]$ where 1 indicates that the entire power used by the PPU is provided by the battery and 0 that it is entirely provided by the electric generators. When negative it indicates that the electric generator is used to re-charge the battery while providing also any electric power required by the rest of the propulsive system.

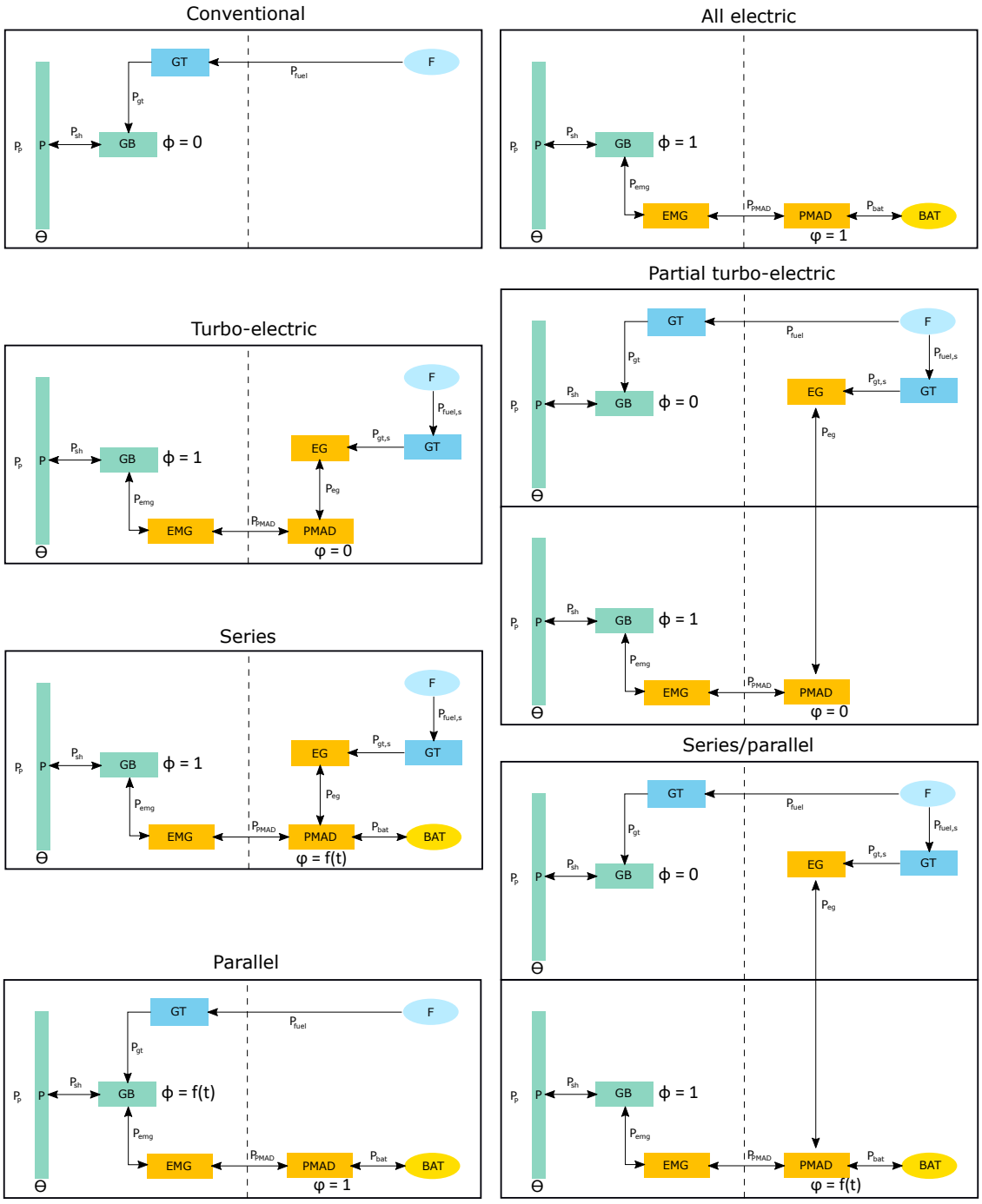

Fig. 3 Simplified models of hybrid electric propulsive system architectures

C. Constraint Analysis

Performance constraint analysis is commonly used at the start of the conceptual design phase to obtain values of the wing and power loading such that requirements derived from the customer and legislation are satisfied by the resulting design [12]. The requirements are represented by curves on a diagram with power-loading (or thrust to weight ratio) on the y-axis and wing-loading on the x-axis. These curves form the boundaries of the feasible design space. In the case of hybrid electric aircraft, the power-based constraint diagram is preferred to the thrust based one as the internal components of the powertrain are sized with respect to power requirements.

The constraint curves are either derived from statistical data or by solving the system of forces acting on the aircraft modelled as a point such that it is in equilibrium. Constraints along the aircraft vertical axis results in boundaries that indicate the maximum wing loading (i.e. smallest wing area per unit of mass) allowable. Solving the equilibrium system along the longitudinal axis provides curves that can be solved for the propulsive power loading as a function of wing loading, atmospheric conditions and other aircraft performance parameters.

The propulsive power results are valid for conventional and hybrid electric designs alike since the underlying assumption of equilibrium of forces over a point is detached from any definition of the propulsion system architecture. However, the thrust power loading needs to be further corrected before it can be used as a parameter in the sizing procedure. Specifically, it needs to be converted to shaft power loading by considering the following corrections:

- Aero-propulsion system interactions
- Propulsive efficiency
- Atmospheric and flight speed conditions
- One Engine Inoperative (OEI) conditions

These corrections are influenced by the chosen propulsion system architecture and as such, benefits to the final design can be obtained when propulsive system hybridization is used. Figure 4 illustrates what could be expected when the corrections dependant on the choice of propulsive system architecture are taken into consideration for the derivation of the wing and power-loading characteristics.

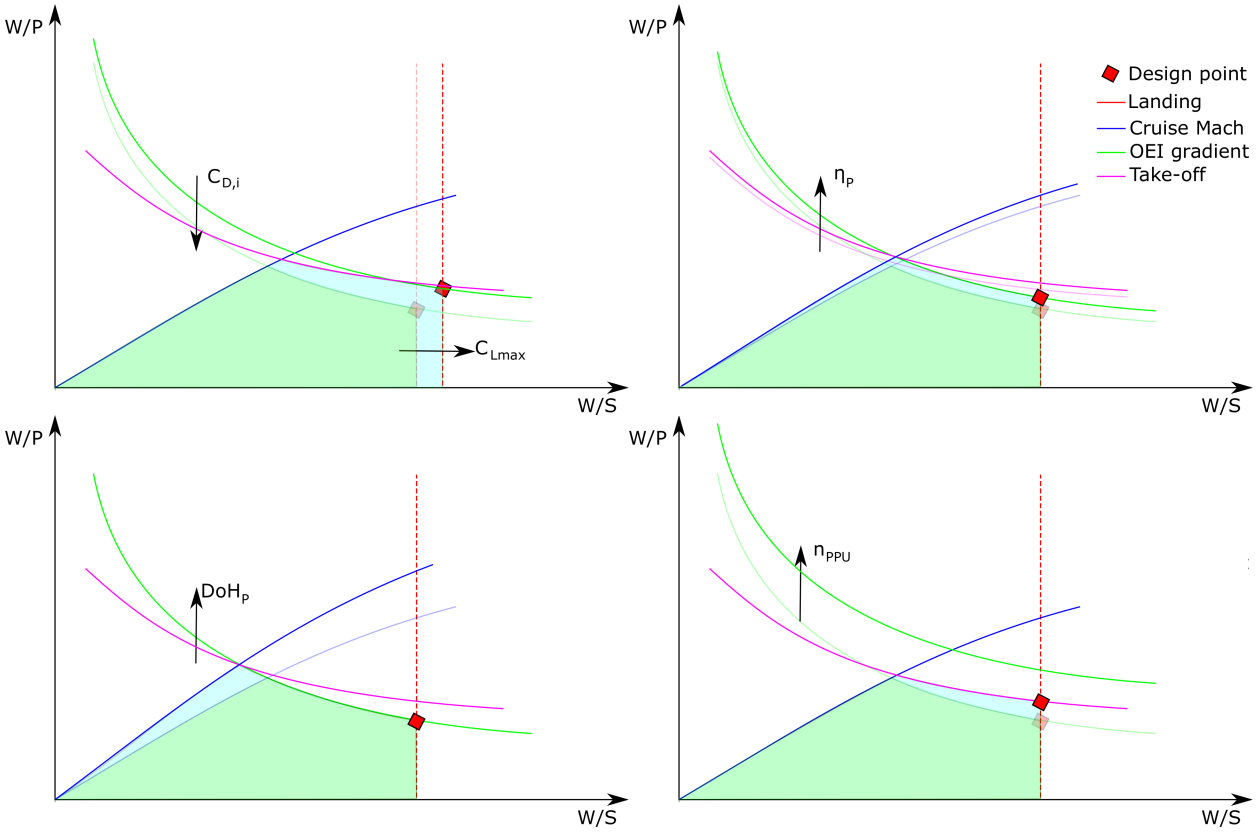

Fig. 4 Effects of corrections on power-loading constraint diagrams. Top-left: aero-propulsive changes. Top-right: propulsive efficiency correction. Bottom-left: altitude/power-lapse influence. Bottom-right: number of PPU effect.

1. Aero-propulsive Interaction Correction

Among the many reasons why the electrification of the propulsion system is deemed interesting there is the possibility to take advantage of beneficial interactions between the aircraft aerodynamics and propulsion. Propulsion integration strategies that could benefit from the use of electric motors are many. For example, using distributed propulsion to

enhance the wing lift [13, 14], using small propellers to reduce the wing tip swirls thus reducing the lift induced drag [15] or taking advance of the high controllability of the electric motors to produce differential thrust and reduce the vertical tail area requirement for yaw stability and control [16].

All these interactions are based on very complex phenomena that are difficult to model at the conceptual design stage and they are outside the scope of this work. However, it is understood that the possible benefits are a main driver in the choice of propulsive system architecture so in this work, assumptions on the magnitude of these effects are derived from relevant studies and used in the form of correction factors in the computation of the aircraft lift-drag characteristics and propeller efficiency. These changes impact both the constraint and point mass analysis.

2. Propulsion Efficiency Correction

The propulsive power loading that results from the equilibrium in the longitudinal axis is not yet usable for the sizing of the propulsive units as it does not consider the losses at the thrust-producing device. In case of a turbo-prop aircraft, the mechanical power at the shaft is transformed into usable thrust by a propeller. The losses of this conversion are captured in the propeller efficiency defined as the ratio between the propulsive and shaft powers:

$$\eta_{\mathrm{P}} = \frac{P_{\mathrm{P}}}{P_{\mathrm{sh}}} = \frac{T \cdot V}{P_{\mathrm{sh}}} \tag{4}$$

Similarly to the user defined changes to lift and drag coefficient, it is possible that a certain propulsion system architecture allows an increase to the overall propulsive efficiency. Improvements derived in this way are expected to be relatively small as the baseline study case uses already very efficient turbo-propeller propulsion while larger improvements could be obtained in turbo-fan propulsive devices [17]. Nevertheless, if changes to the propulsive efficiency are expected when selecting a configuration, they can be integrated with constraint and segment-specific correction factors.

3. Power Lapse Correction

The impact of the atmospheric conditions on the power requirements is captured in the power lapse coefficient. This is defined as the shaft power at altitude over the sea-level-static power that would be produced by the machine with the selected throttle settings:

$$\Upsilon = \frac{P_{\mathrm{sh,\,gt}}}{P_{\mathrm{sh,\,gt,\,0}}} = \left(\frac{\rho}{\rho_0}\right)^k \tag{5}$$

Where ρ is the air density at altitude, ρ_0 is the ISA air density at 0 meters and k is a coefficient that depends the machine characteristics, the flight altitude and flight Mach number. These characteristics are complex to fully model, so they can be provided through a performance map or by using experimentally derived factors as proposed by Ruijgrok in [18].

A main difference exists between air-breathing and electrical machines. The former sees a degradation of performance as altitude increases due to the reduction of air density that negatively impacts the engine's mass flow rate. This phenomenon is partially counterbalanced by the improvement of the specific thrust/power due to lowering of the inlet temperature leading to an estimated correction coefficient k of 0.75. On the other hand, electric motors are very weakly influenced by changes in atmospheric conditions, so they can be modelled as having a correction coefficient k equal to 0. The net result is that the power-lapse correction needs to account for the segment degree of hybridization to correctly introduce the effects of altitude to the constraint and mission analysis as defined in Equation 6:

$$W/P_{\mathrm{sh,\,0}} = \frac{W/P_{\mathrm{sh,\,gt}}}{\Upsilon} + W/P_{\mathrm{sh,\,em}} = W/P_{\mathrm{sh}} \cdot \left(\frac{1 - DoH_{\mathrm{P,\,seg}}}{\Upsilon} + DoH_{\mathrm{P,\,seg}}\right) \tag{6}$$

Where $DoH_{\mathrm{P,\,seg}}$ is the ratio between electric and total shaft power at altitude as defined in Equation 7. This parameter changes depending on the segment considered as different amount of electric power could be used along the mission.

$$DoH_{\mathrm{P,\,seg}} = \frac{P_{\mathrm{sh,\,em}}}{P_{\mathrm{sh}}} = \sum_{\mathrm{i}=1}^{n_{\mathrm{PPU}}} \left(\frac{P_{\mathrm{sh,\,i,\,em}}}{P_{\mathrm{sh,\,i}}} \cdot \frac{P_{\mathrm{sh,\,i}}}{P_{\mathrm{sh}}}\right) \tag{7}$$

It can be observed that a higher electrification has a beneficial impact on the aircraft characteristics as long as the altitude-based constraints are the sizing the power-lapse requirements.

4. One Engine Inoperative Correction

Certain critical requirements need to be satisfied even if one of the PPU fails. Therefore, the obtained shaft power loading needs to be further corrected for OEI conditions to ensure that the remaining powerplants can provide enough thrust to maintain a safe flight condition.

In a conventional aircraft, the propulsive units are typically all the same dimension since having different engines would increase the acquisition and maintenance costs. With thrust equally produced by all propulsive devices, the most critical condition becomes the one in which the engine further away from the fuselage centre line fails as this produces the highest yaw moment. In this case the OEI power loading correction factor is simply:

$$k_{\mathrm{OEI}} = \frac{n_{\mathrm{PPU}} - 1}{n_{\mathrm{PPU}}} \tag{8}$$

However, the hybridization of the powertrain enables the option to distribute the thrust in different ways that can lessen the impact of a propulsion machine failure. When distributing the thrust in a heterogeneous way the correction factor becomes function of the largest propulsive power unit:

$$k_{\mathrm{OEI}} = \frac{P_{\mathrm{P}} - max\left(P_{\mathrm{P,\,i}}\right)}{P_{\mathrm{P}}} = 1 - max\left(\Theta_{\mathrm{i}}\right) \tag{9}$$

If parallel PPU are used in the design (i.e. the propeller shaft is driven simultaneously by a conventional engine and an electric motor), it could be argued that not all power at the propeller shaft would be lost if one of the two machines fail. Therefore, the designer needs to indicate if a total or partial PPU failure is expected. Clearly, the latter option lessens the OEI constraint severity, so it should be chosen under the assumption that the regulations would permit the fulfilment of the requirements in this way.

The failure of one of the PPUs does not only diminish the maximum thrust that can be produced by the propulsive system, but it has consequences on the aircraft aerodynamics as well in the form of an increased drag. This increase is due to the wind milling of the propeller and due to an increase of trim drag caused by the necessity to offset the moment generated around the aircraft vertical axis from the non-symmetrical thrust distribution. The increase in drag is considered in the sizing method using the increment factor $\Delta C_{\mathrm{D,\,OEI}}$ when the drag polar is needed in the computation of the constraint Equation.

D. Point Mass Analysis

Once a prediction of the total shaft power loading and wing loading are computed by the constraint analysis module, the mission analysis is initialized. The mission module implemented in Pacelab APD * allows the user to create a flight profile by connecting an arbitrary number of segments. Each segment has its own flight performance computation routine and when its estimation is completed its results are propagated downstream to the following objects.

1. Propulsive Device and Thrust Computation

The constraint and mass point analysis require a model for the efficiency of the propulsive device to translate a propulsive power requirement into its shaft power counterpart. The propulsive device of choice in this study is a high-speed propeller such as the ones used in modern turbo-props. It is necessary that the propeller performance is sensitive to changes in flight altitude and state to fully capture the operational requirements that needs to be satisfied by the propulsive system. However, the propeller model should not be too complex/slow as it will be called by the solver thousands of times per solution iteration. It should also work for a wide range of thrust setting, device dimensions and speeds as the overall aircraft geometry can quickly change during the conceptual design phase. The Actuator Disk Theory was therefore chosen as it requires few inputs that are easily parametrizable and it offers fast solution while still being able to capture the impact of altitude and speed on the propeller efficiency. This efficiency is defined as:

$$\eta_{\mathrm{P,\,th}} = \frac{2}{1 + \sqrt{1 + \frac{T}{\frac{1}{2}\rho\frac{\pi}{4}D^2V^2}}} \tag{10}$$

*Pacelab APD is a commercial software created and distributed by the company PACE that is meant to offer a fully-fledged preliminary aircraft design environment that allows users to model, analyse and optimize aircraft configurations and system architectures. The presented work is implemented in a custom-defined instance of the software.

Where the subscript *th* denotes that this is the theoretical upper limit attainable as this model does not account for losses due to non-uniform axial velocities and residual rotational kinetic energy. This makes the model inaccurate at lower speeds where these effects are most accentuated. In order to use the propeller efficiency defined in Equation 10 a correction factor is introduced. Sources report the theoretical propeller efficiency overestimates the actual efficiency by 15 to 10% in climb and cruise conditions while the error grows up to 50% when the aircraft is stationary [18]. Therefore the correction coefficient k_{prop} (function of the advance ratio J) is introduced such that the efficiency reflects these numbers:

$$\eta_{\text{P}} = \frac{P_{\text{P}}}{P_{\text{sh}}} = k_{\text{prop}} \cdot \eta_{\text{P, th}} \tag{11}$$

The propeller diameter is computed from the disk loading input defined as the ratio between the shaft power and propeller area in order to ensure that the propeller dimensions change alongside the PPU during the sizing process.

2. Propulsive System Reference Power Computation

Once the required propulsive power and efficiency are known, the sizing requirement for the gearbox of a specific propulsive power unit becomes simply the maximum value computed during the sizing mission:

$$P_{\text{gb}} = \Theta_{\text{i}} \frac{P_{\text{P}}}{\eta_{\text{P}}} \tag{12}$$

The rating shaft powers of the electric motor and gas-turbine engine are derived using the *shaft power ratio* and considering the gearbox efficiency so that any mechanical losses due to the gearing system are represented in the power and energy estimations.

$$P_{\text{em}} = \varphi \frac{P_{\text{gb}}}{\eta_{\text{gb}}} \tag{13}$$

$$P_{\text{gt}} = \Upsilon \left(1 - \varphi\right) \frac{P_{\text{gb}}}{\eta_{\text{gb}}} \tag{14}$$

The gas turbine shaft power is also further corrected with the use of the power lapse Υ as defined in Equation 5.

The fuel flow required by the gas turbine is computed as a function of the control setting and flight state (Mach, temperature and altitude) using a fuel flow map. The fuel power can then be derived by considering the fuel specific energy ϵ_{fuel} or defined as a function of the gas-turbine power using the machine efficiency:

$$P_{\text{fuel}} = \epsilon_{\text{fuel}} \dot{m}_{\text{fuel}} = \frac{P_{\text{gt}}}{\eta_{\text{gt}}} \tag{15}$$

On the electrical power-path, the power drawn by the electric motors is provided by the Power Modulation and Distribution (PMAD) sub-system:

$$P_{\text{PMAD}} = \frac{P_{\text{em}}}{\eta_{\text{em}} \eta_{\text{cb}}} \tag{16}$$

The PMAD is used as a simplification of the complex electric system since, depending if the power is provided by alternating or direct current, there is the need to connect a different number of electrical components such as inverters, rectifiers, transformers and circuit breakers. The electric components are not perfectly efficient when transferring energy so the PMAD needs to take these losses into account. As suggested in reference [4], the overall efficiency of the PMAD can be defined as the product of the n electric components connected in series:

$$\eta_{\text{PMAD}} = \prod_{\text{i=1}}^{n} \eta_{\text{ec, i}} \tag{17}$$

Where the component electric efficiency is assumed variable with the required power as the nominal conversion ratio drops off when not under full-load due to internal losses that are independent of the load.

Then, the power required by the gas turbine connected to the electric generator becomes:

$$P_{\text{egt}} = \Upsilon \left(1 - \phi\right) \frac{P_{\text{PMAD}}}{\eta_{\text{eg}} \eta_{\text{cb}} \eta_{\text{PMAD}}} = \Upsilon \frac{P_{\text{eg}}}{\eta_{\text{eg}}} \tag{18}$$

And the power drawn from the battery is:

$$P_{\text{bat}} = \phi \frac{P_{\text{PMAD}}}{\eta_{\text{bat}}\eta_{\text{cb}}\eta_{\text{PMAD}}} = \frac{P_{\text{bat, out}}}{\eta_{\text{bat}}} \tag{19}$$

As this gas turbine and the battery pack are in the system side of the propulsive power unit, their nominal power and fuel mass flow depend on the sum of all the power requirements at a point in time. If more than one gas-turbine and battery packs are in the design, the user indicates how much of the power or energy requirement is taken upon by the single object. This also becomes useful to ensure that the power sources are sized regarding safety standards using redundant and over-sized critical components.

3. Energy Sizing and System Efficiency

Once the total fuel and battery powers are known, the overall propulsive system efficiency can then be defined as the ratio between the propulsive power and total supply power drawn from the sources [17]:

$$\eta_{\text{ov}} = \frac{P_{\text{P}}}{P_{\text{bat}} + P_{\text{fuel}}} \tag{20}$$

This value is an interesting parameter for hybrid powertrains as the electric side has overall better performances, so it is expected that with an increase of hybridization, the power conversion between sources and users would happen with fewer losses possibly leading to lower energy consumed for a given mission.

The energy requirement during a flight segment sub-divided in n time-steps is computed using the Riemann trapezoidal sum:

$$E_{\text{fuel}} = \sum_{\text{i=1}}^{n} \left[\left(\frac{\dot{m}_{\text{fuel, i}} + \dot{m}_{\text{fuel, i-1}}}{2} \right) \cdot \epsilon_{\text{fuel}} \cdot (t_{\text{i}} - t_{\text{i-1}}) \right] \tag{21}$$

$$E_{\text{bat}} = \sum_{\text{i=1}}^{n} \left[\left(\frac{P_{\text{bat, i}} + P_{\text{bat, i-1}}}{2} \right) \cdot (t_{\text{i}} - t_{\text{i-1}}) \right] \tag{22}$$

If an electric battery is fully discharged it can become irreparably damaged and its performance deteriorates. Therefore, depending on the battery chemistry and level of technology assumed, the designer should indicate the maximum degree of discharge allowable so that the tool can oversize the battery mass accordingly.

Finally, the authors of reference [19] suggests the use of two parameters to allow a quick understanding of the operational use of the electric side of the hybrid system. These are the power and energy degrees of hybridization:

$$DoH_{\text{P}} = \frac{P_{\text{em}}}{P_{\text{em}} + P_{\text{gt}}} \tag{23}$$

$$DoH_{\text{E}} = \frac{E_{\text{bat}}}{E_{\text{bat}} + E_{\text{fuel}}} = \frac{E_{\text{bat}}}{E_{\text{tot}}} \tag{24}$$

This marks the end of the point mass analysis procedure. The energy and power requirements are then translated into masses and dimensions by the aircraft sizing module. Conventional machines and other structures of the aircraft (fuselage, wing, landing gear etc.) are sized with the use of conceptual design procedures previously implemented in Pacelab APD derived from the work of Torenbeek [20] and Raymer [12]. The electric components (battery pack, motors, generators, PMAD and cabling system) are sized with components specific rules as described in the full report of this work [10].

III. Sample Application Results

The results presented in this section have been obtained using the previously presented method adopting an ATR72 as the reference design as described in subsection III.A and using technology level assumptions as presented in subsection III.B.

Three architecture morphologies have been selected in order to show the flexibility and adaptability of the proposed procedure when considering a wide range of hybrid electric solutions. These are presented in subsection III.C.

A series of response surfaces have been obtained in order to understand how the three control parameters influence the results and to identify a starting point for a more localised optimisation. The resulting response surface are shown and discussed in subsection III.D. Then, a starting point is chosen for each of the three designs taken into consideration and the results are discussed in subsection III.E.

A. Mission Requirements

An ATR72-600 has been chosen as the reference and starting point for this work as it is a successful aircraft in the regional market and its characteristics are easily found in the literature simplifying the tool validation and calibration. This design has also been previously chosen as the reference in similar works (e.g. [21–23]) thus allowing an easier comparison of the results presented below.

The harmonic mission (including reserves) used for the sizing procedure is reported in table 1. These requirements are kept constant in the rest of the study, so the proposed designs can be compared in terms of effectiveness in accomplishing the mission.

Table 1 Harmonic mission parameters for baseline design.

Harmonic Mission		
Passengers	70 (@95kg/PAX)	PAX
Payload	7500	kg
Mission range	1530	km
Cruise altitude	5500	m
Cruise Mach	0.43	Mach
TOFL	1333	m
LFL	1067	m
Taxi	4+4	min
Reserves		
Diversion range	182	km
Diversion altitude	3000	m
Diversion speed	0.4	Mach
Hold time	30	min

Further operational characteristics are also kept constant for the study. Take-off and landing fields are assumed at ISA conditions at 0 m. Climb is conducted at constant CAS up to 3000 m and then the aircraft speed is increased up to cruise Mach of 0.43. The cruise segment is carried out at constant altitude as the optimal trajectory is function of the hybridization ratio and control strategy, further increasing the complexity of the analysis. Optimizing the cruise segment could be an interesting study once a configuration has been identified. A 1000 fpm constant descent rate is then set to decrease the altitude during the descent phase as suggested in [18].

B. Technology Maturity Level Assumptions

In the method proposed, the mass of each component in the HEP system is derived from the reference power (or energy) computed during the point mass analysis and sizing parameters such as gravimetric specific power. Table 2 shows the main parameters used in this study. As the results are sensitive to these assumptions, the one about the battery characteristics, two maturity levels have been identified to carry out the design space exploration.

Both assumptions shown in table 2 are for an expected year into service of 2035-2040 but show two different estimations for what the technology of electric components will achieve. For both assumptions levels, the cabling system characteristics are the one of modern high-power aluminium cables as the use of super-conductive cryogenic power lines is seen as a technology still in its infancy by many authors [4] making their use not suitable for the required YEIS. The conservative estimations for motors, generators and electric components are not far from what could be achieved soon with state-of-the-art technologies. On the other hand, the more optimistic assumption is close to what is normally regarded as the limit of non-superconductive machines.

When looking at the assumptions for the battery, even the most conservative estimation for the specific energy is double of what is possible with today's best lithium-ion cells and it also exceeds the theoretical limit for this chemistry. However, lithium-sulphur cells could bridge the gap in the required time-frame [24, 25]. The second assumption for the cell specific energy sets a target of 750 Wh/kg, a very optimistic assumption that exceeds even the capability of lithium-sulphur and would be achievable only with technologies such as lithium-air.

Table 2 Technology level assumptions for the design space exploration.

Input	Symbol	Unit	Conservative	Optimistic
Electric motor/generator specific power	$\varrho_{em}/\varrho_{eg}$	[kW/kg]	5/12	9/20
Electric motor maximum efficiency	η_{em}	[%]	95	95
Electric component specific power	ϱ_{ec}	[kW/kg]	9	15
Electric component efficiency	η_{ec}	[%]	90	95
Cable conductor density	$\rho_{cb,\,co}$	[g/cm^3]	3.3	3.3
Conductor resistivity	σ_{cb}	[$\Omega \cdot$ mm^2/m]	$3.7 \cdot 10^{-2}$	$3.7 \cdot 10^{-2}$
Conductor design current density	j	[A/mm^2]	2.5	2.5
Battery specific power	ϱ_{bat}	[kW/kg]	0.6	0.8
Battery specific energy	ϵ_{bat}	[Wh/kg]	500	750
Battery maximum efficiency	η_{bat}	[%]	85	90
Battery minimum State Of Charge	SOC_{lim}	%	20	20

C. Hybrid Electric Configurations

Among the many hybrid propulsive system architectures proposed in the past, three exemplary ones have been chosen to show the flexibility of the methodology proposed. These architectures have been selected as they can be completely defined with the use of only one of the three control parameters proposed in this study. Therefore, any other architecture would result from a mix of the ones presented below.

1. Parallel Architecture

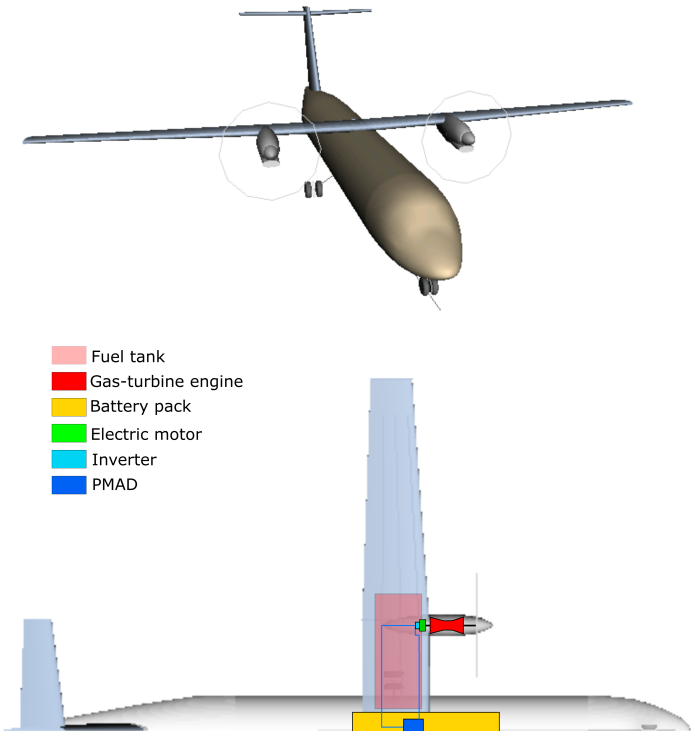

Fig. 5 Parallel hybrid electric architecture external and internal configurations.

The first architecture considered is characterized by two wing-mounted parallel PPU providing power to the propellers. Th external and internal propulsive system architecture morphologies are shown in Figure 5. For this specific PPU, it is

expected that the electric motors would be directly connected on the engine or gearbox shafts. They provide part of the required shaft power using only the energy stored in the battery packs as no generator is present in this specific architecture. The electric power ratio, ϕ, is set to 1 and kept constant throughout the mission. Moreover, the symmetry of the two PPU means that the propulsive power share, Θ, of each PPU is set to 0.5. Therefore, the only free parameter is the shaft power ratio, φ, that can be varied between 0 (propeller driven by engine only) to 1 (propeller electrically driven).

2. Parallel/Series Architecture

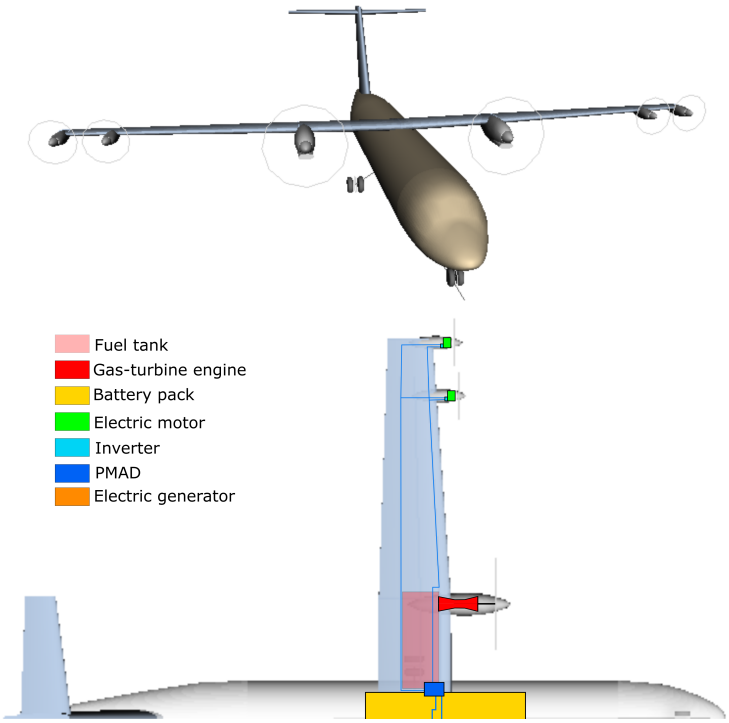

Fig. 6 Parallel-series hybrid electric architecture external and internal configurations.

In Figure 6, the second architecture used in this study is shown. This design uses conventional turbo-prop PPU on the inboard part of the wing and a pair of electrically driven propellers at the wing-tip. Similar designs have been proposed by DLR [23], NASA [26] and in other studies [22].

The tip-mounted propellers have been chosen as improvements in terms of propulsive efficiency and wing performance can be achieved as described in references [27]. The interaction between propeller, motor nacelle and wing-tip are complex effects that depend on a multitude of factors such as the wing geometry (e.g. the aspect ratio), the lift coefficient, its distribution along the span and the strength and direction of the propeller swirl [28, 29]. As the performance improvements are the main driver behind the choice of the propulsive system external morphology, an improvement of the propeller efficiency of 18% has been used as proposed in reference [26] where a similar design was presented.

The internal architecture of the parallel/series design is shown in the bottom part of Figure 6. It can be observed that the inboard gas-turbine engines are providing power to the inboard propellers while no connection with the electric side of the propulsive system exists. To obtain this architecture, the inboard PPU is characterized by a constant shaft power ratio of 1, while the outboard PPUs are characterized by a shaft power ratio of 0 (fully electric shaft) and electric power ratio of 1 (fully battery powered). Therefore, the degree of hybridization of this design and the usage of electric energy as function of mission time are fully controlled by changing the relative power provided by the PPUs using the propulsive power share parameter.

3. Distributed Series Architecture

The third design proposed for this study is shown in Figure 7 and is characterized by the distribution of the propulsive power over ten identical electrically driven propellers positioned along the entirety of the wing span. This configuration is often presented alongside the use of electric technologies as conventional gas-turbine engine scales poorly (i.e. their thermal efficiency decreases with smaller dimensions); on the other hand, electric motors are highly scalable without substantial penalties.

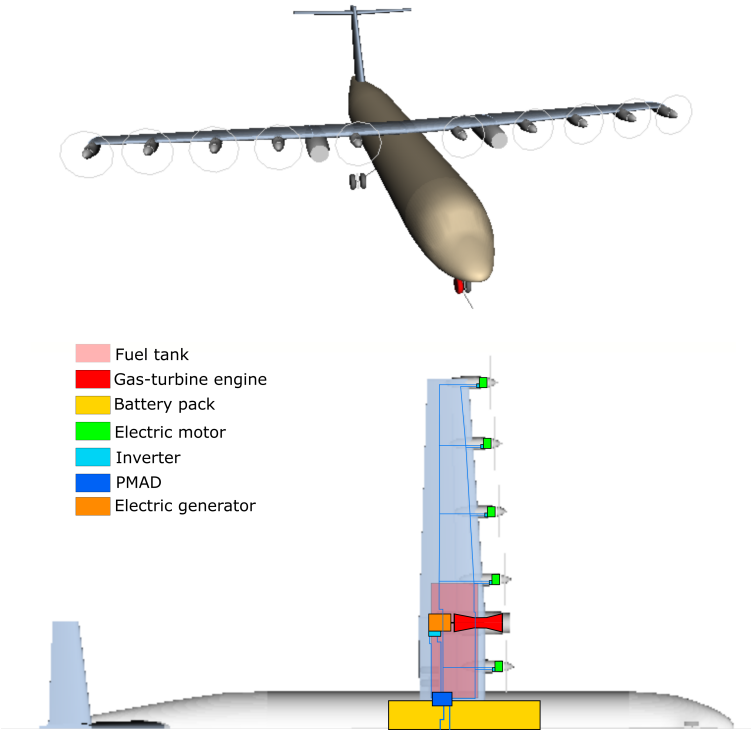

Fig. 7 Distributed series hybrid electric architecture external and internal configurations.

Existing studies on DEP tend to focus on the aero-propulsive characteristics of the concept while neglecting the impact of the propulsive system internal architecture. This is mostly because it is often assumed that the design would be fully electric. However, in this study it is assumed that only part of the required energy is supplied by batteries. The remaining requirement is instead produced by electric generators connected to air-breathing engines as shown in the bottom of Figure 7.

Placing a lifting surface in the accelerated flow behind a thrust producing propeller can increase its lift and profile drag [14, 23]. This effect is more pronounced during low-speed segments when the relative increase of dynamic pressure is larger. The disposition of the PPUs in this design is chosen so that the region of wing immersed in the slip-stream is maximized thus taking advantage of the increased lift capabilities to reduce the required wing area (i.e. increasing the maximum allowable wing loading) leading to a lighter wing that will generate less drag during high-speed segments. The main drawback is that the lift is coupled to the thrust setting, making the control of the aircraft more difficult and the design less safe in case of propulsion system failures.

The effect of the propellers has been modelled by assuming segment specific correction factors for the aircraft lift-polars derived by previous works [13, 14, 23, 30]. These are a +15% increase of the maximum lift coefficient, $C_{l,\,max}$, in take-off conditions and a lower improvement of 10% during landing as using full-thrust would not allow for the required deceleration in this phase. To account for the more turbulent flow hitting the wing, the parasitic drag coefficient has been increased by a factor of +10% during these segments.

To define this architecture using the proposed method, the only parameter that is needed is the electric power ratio, φ, controlling the power provided by the generators and battery packs at any given time in the mission. The lack of conventional machines directly connected to the propellers means that the shaft power ratio is set permanently to 0 while the assumption that the ten propellers are identical leads to a constant propulsive power share of 0.1 for each PPU.

D. Design space exploration

The control laws used in the definition of the propulsive system morphology could be specified at segment level in order to allow complex strategies such as moving the sizing requirement for the engines from the take-off to the cruise condition while providing the rest of power by electric means. However, the parameters are initially grouped in two sets characterized by high-power (take-off and climb) and low-power requirements (cruise, descent, landing, taxi). In this way, response surfaces for a series of key performance indicators can be shown and used to get a better understanding of the impact of the control strategy on the three configurations.

The Degree of Hybridization on the x and y-axis of the following figures should be read as a general indication of the free control parameter that changes depending on the architecture considered (i.e. a DoH of 1 equal to a $\phi = 1$ for the parallel design, a $\Theta = 0$ for the hybrid configuration and to a $\varphi = 1$ for the distributed series design). The contour map indicates the relative change of the considered value using as reference the results of the baseline design (an ATR72 aircraft). The reference data used here can be found in the first column of table 3.

To facilitate the reading of this chapter, only the response surfaces resulting from the design space exploration for the MTOW, fuel mass and ESAR changes are shown. The resulting maps for other important indicators such as total energy, overall system efficiency and well-to-propeller CO_2 emissions are omitted due to space limitation but can be found in the complete work on which this paper is based at [10].

1. MTOW results

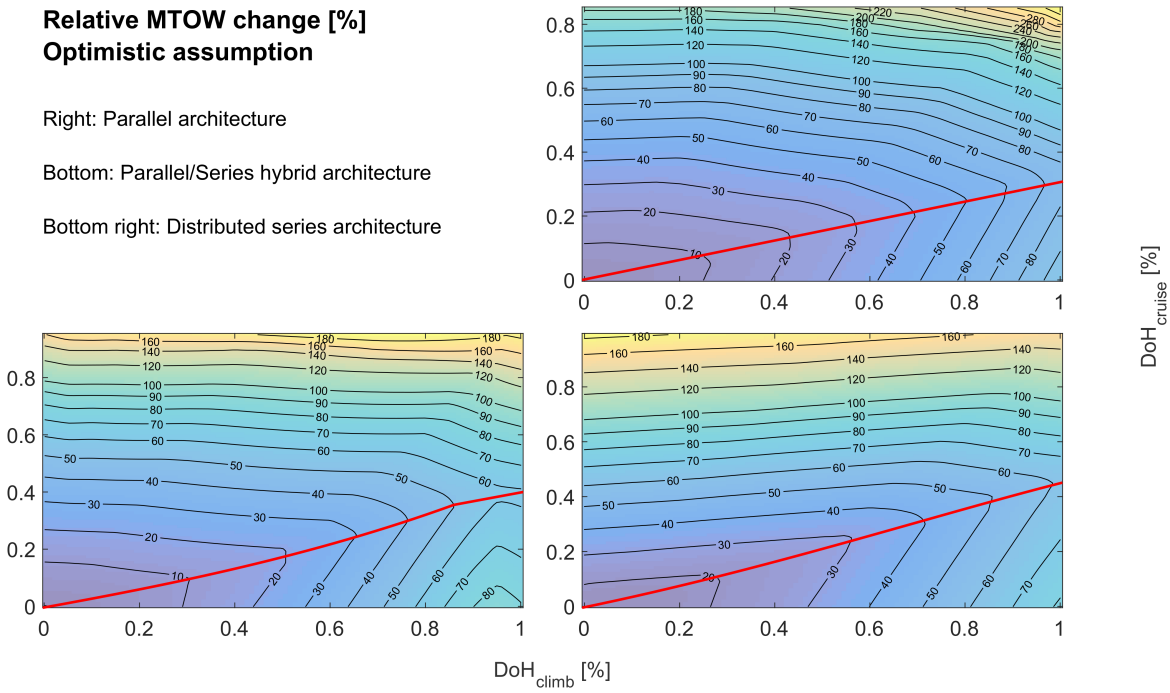

Fig. 8 MTOW change as a function of the control parameters and optimistic assumption.

The first Key Performance Indicator taken into consideration is the MTOW of the design. Figure 8 shows the resulting response surfaces for the three architecture morphologies. Only the optimistic level assumption is reported for the mass changes as the conservative assumption results show the same trend, albeit with a quicker increase in MTOW (about 15 to 25% higher MTOW at any given point in the map) as the design become more electric.

For all three architectures, the resulting contour maps show that the MTOW is expected to increase as the overall degree of hybridization is increased. Two distinct regions are separable as highlighted by the red line cutting the maps diagonally. The upper region shows that the MTOW has a high sensitivity to the cruise DoH while it sees little or even positive influence with increasing climb DoH. This behaviour is due to the battery poor gravimetric energy density when compared to the fuel counterpart. On the other hand, the weak influence of the climb DoH shows that, for a given battery mass, substituting part of the conventional propulsive system with electric machines does not have a large impact

as the specific power of these systems are comparable when their efficiencies are also considered.

In the region below the overlain line, the trend is reversed. An increase of climb DoH leads to a rapid increase of aircraft mass while an increase of battery energy requirement (higher cruise DoH) reduces the design MTOW. This is because the red line highlights the switch in battery sizing from the energy requirement to the peak power that could be drawn during the mission. Thus, the decrease in MTOW as the cruise DoH increases is just the result of substituting fuel for the electric energy already present in an oversized battery.

2. Fuel mass results

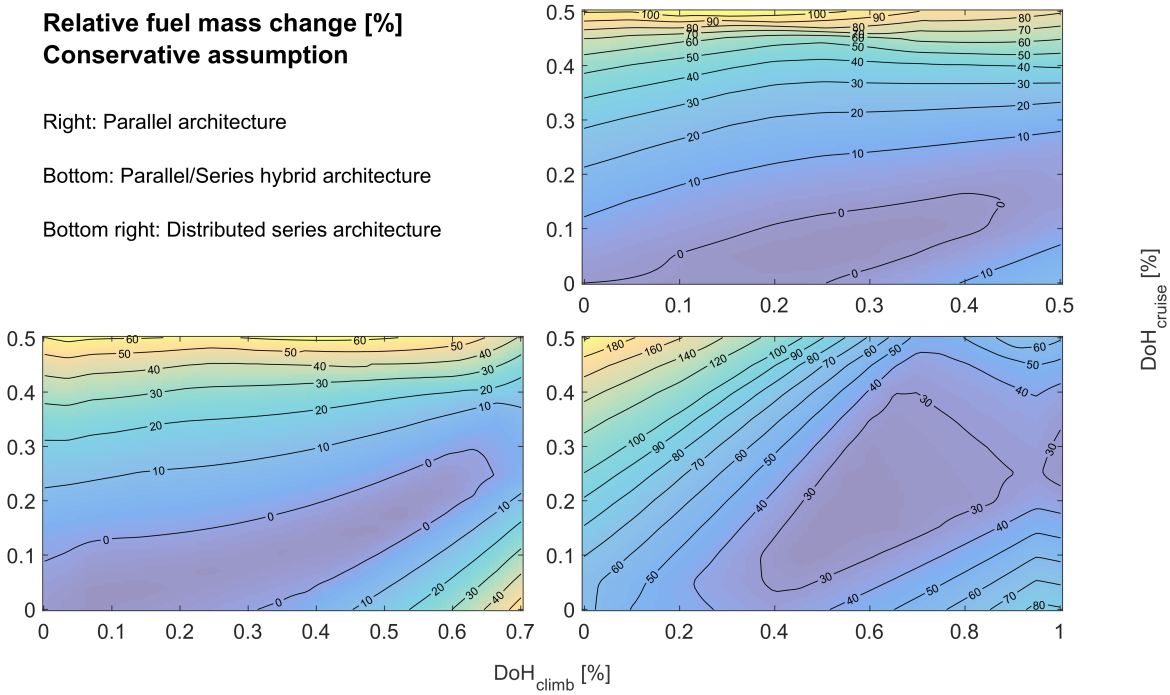

Fig. 9 Fuel response surface for the three HEP architectures. Conservative assumption.

It can be expected that as the overall degree of hybridization of a design is increased, the fuel mass required to accomplish the design mission would decrease as more and more energy is supplied through the electric system. This would be true if exchanging fuel energy for electric energy would not have such a large impact on the aircraft mass. Alas, the results shown in Figure 9 indicate that for the parallel and series/parallel designs only small reductions of less than 10% can be achieved. In particular, the results indicate that using the electric motors continuously during the cruise phase has detrimental effects on the fuel consumption. Positive results can instead be realized by downsizing the conventional engines towards the cruise power requirement while supplying the difference for take-off and climb with the motors.

On the other hand, the distributed series architecture fares much worse since even the best combinations of inputs show an increase of fuel requirement of more than 20% with respect to the ATR72 reference value. Even without storing any energy in a battery pack, the design is worse than the baseline design as observed in Figure 9 at the point [0,0].

The turbo-electric configuration (fully electric propulsion with fully fuel-based energy storage) needs 65% more fuel to fly the reference mission. This is due to the longer energy conversion chain between fuel and propulsive device when compared to conventional designs as the large number of components in this propulsive system architecture is detrimental to the overall mass and efficiency. Other studies indicate that turbo-electric configurations could become of interest only if super-conductive technologies are extensively used in the design [4, 31].

Figure 10 shows the change in fuel mass as a result of the more optimistic assumption for the technology maturity level. All three proposed designs show a similar trend where the optimum point in terms of fuel consumption is close to the fully electric solution (i.e. the global minimum for fuel requirements). This indicates that for better characteristics of the electric components(in particular of the battery), the improvements due to higher system efficiency outdo the negative changes caused by a higher aircraft mass when looking at the fuel results only. However, using these minima

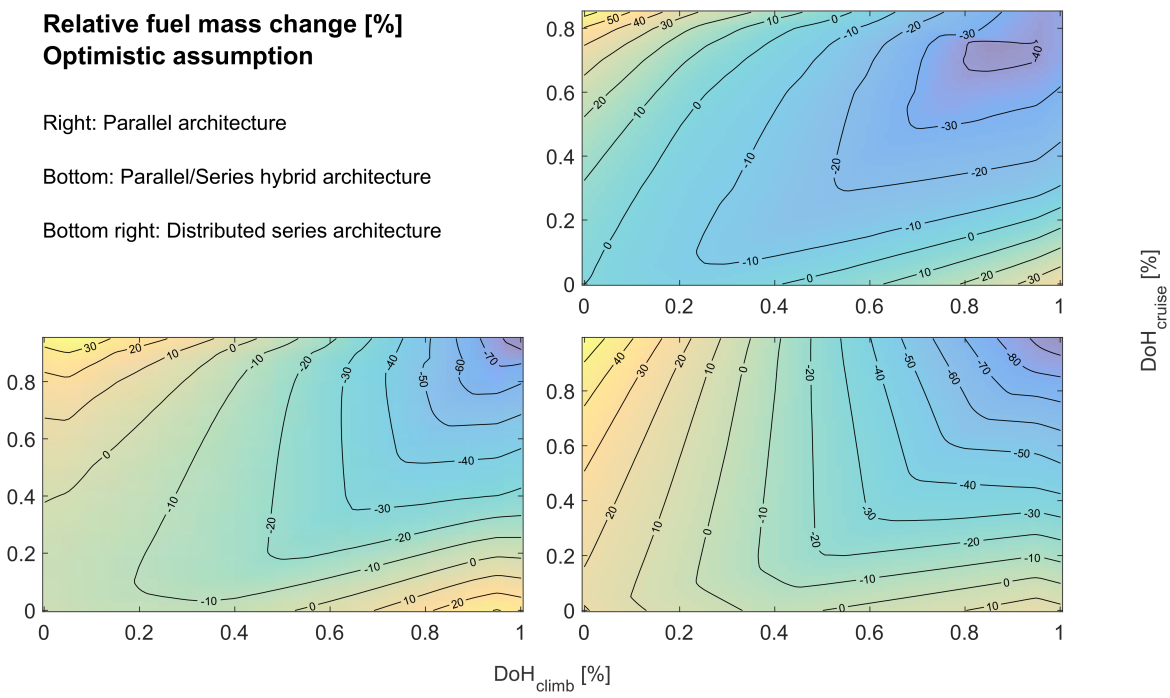

Fig. 10 Fuel response surface for the three HEP architectures. Optimistic assumption.

would lead to 140 to 200% heavier designs than the baseline making them impractical and possibly infeasible when going into more detailed analysis.

3. Energy Specific Air Range results

The reduction of fuel requirement is supported both by airline operators and aircraft regulation agencies as it is directly connected to operational costs and fuel related emissions. However, optimizing a design with only this objective might not be the correct choice as previously shown. A better comparison can therefore be made by considering the total energy (sum of fuel and electric energy) as this allows also the estimations of costs related to the acquisition of electric energy and the emissions related to its production.

Similarly to how the Specific Air Range is used to compare the performances between different designs in terms of distance that can be travelled per unit of fuel consumed, authors of reference [32] have defined the Energy Specific Air Range to allow similar studies with configurations not entirely based on chemical energy storages. The ESAR parameter is defined as the range covered per unit of energy:

$$ESAR = \frac{dR}{dE} = \frac{V \cdot L/D}{TSPC \cdot W} = \frac{\eta_{ov} \cdot L/D}{W} \tag{25}$$

The ESAR proves an interesting value for hybrid electric configurations as it is directly function of the aircraft weight and propulsive system efficiency, two values greatly affected by the use of batteries and electric machines.

Figures 11 and 12 show the contour maps for the time-averaged ESAR for the two technology level assumptions. For low specific energy and power assumptions, only the series/parallel configuration show slight benefits over the baseline results and only for a low degree of hybridization. In particular, the results show that high battery utilization during cruise is not favourable. Exchanging conventional power capabilities for electric ones is the only change that could be leveraged if battery characteristics do not greatly improve.

Figure 12 shows the results for the optimistic assumptions. It is observed that the maximum position for each map is located on the boundary between the power and energy sizing constraints as previously highlighted in Figure 8. This indicates that over-sizing the battery packs either in terms of power or energy has always detrimental outcomes for the overall design performances.

The best control strategy is also greatly influenced by the HEP configuration. The design using two parallel PPUs shows the best improvements for low degree of hybridization using most of the installed electric power and energy to

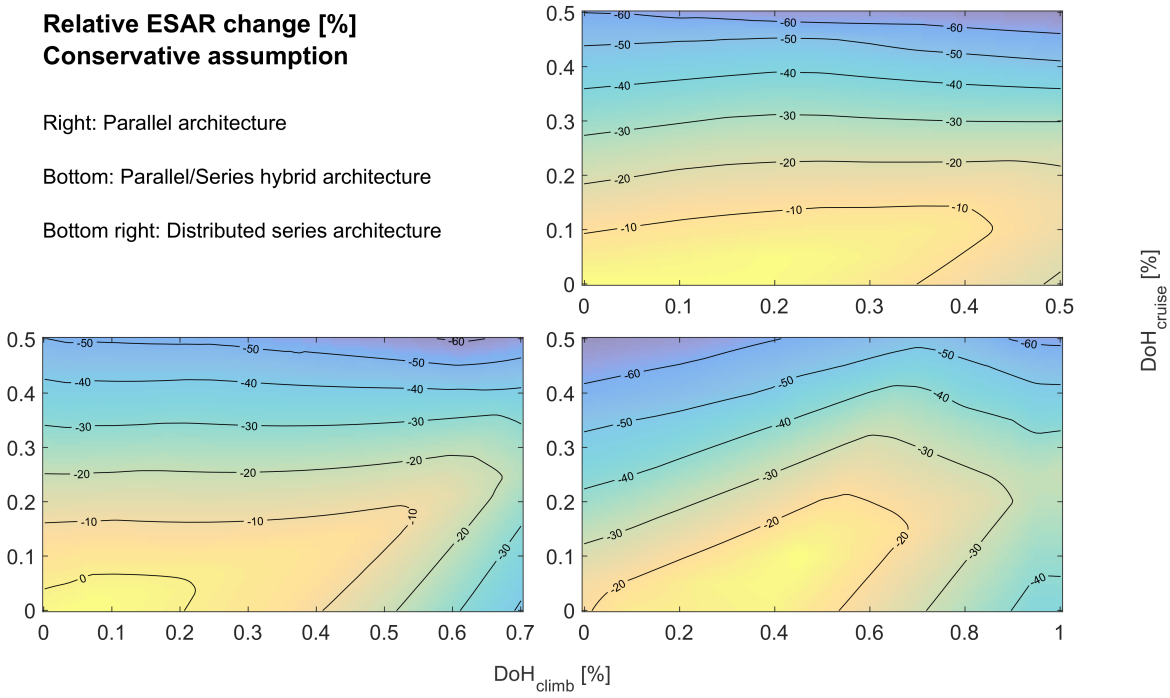

Fig. 11 ESAR response surface for the three HEP architectures. Conservative assumption.

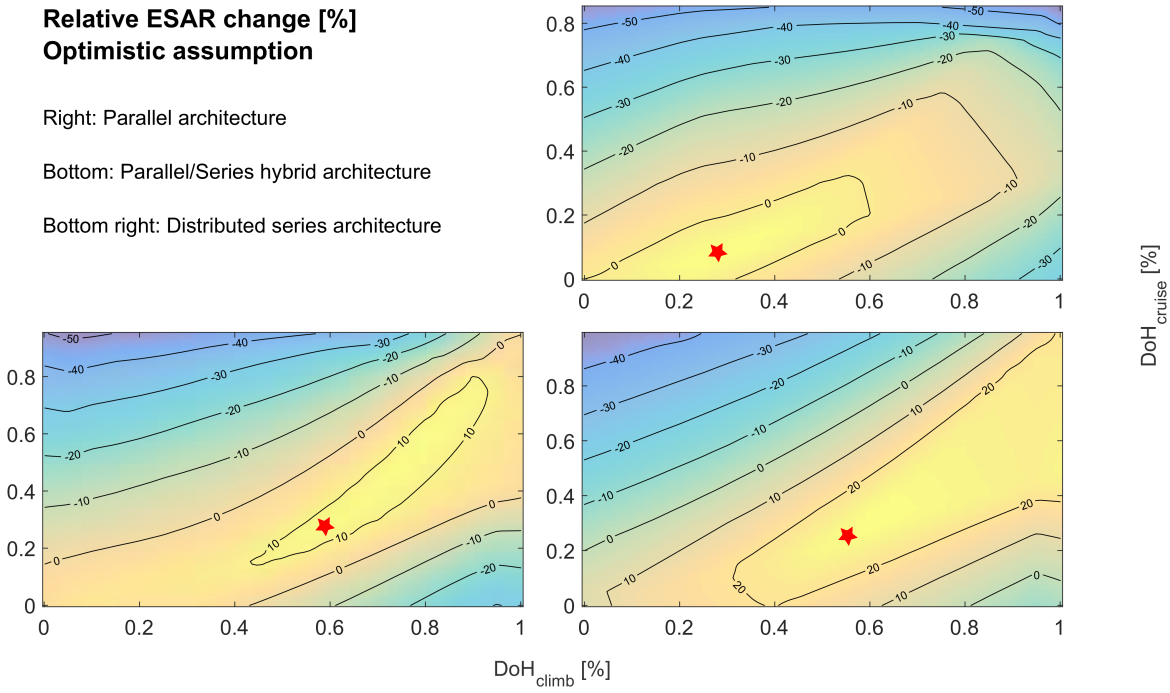

Fig. 12 ESAR response surface for the three HEP architectures. Optimistic assumption.

supply the take-off and climb phases while the cruise segment should be carried out mostly using fuel as the energy source. The other two architectures see their maxima position moved toward more electric solutions in terms of electricity usage during the cruise phase. In this way, the reduction in total energy is higher due to a large decrease of fuel consumption in exchange for a higher aircraft mass.

The conservative assumption trends are comparable to what was found in the work of de Vries et al. [33] where the same baseline design was re-designed with a hybrid electric powertrain. Their study also finds that an increase in mass is to be expected, that little improvement is achievable with engine boosting (parallel architecture) and low DoH, and that the DEP configuration is not a good choice as the increase of propulsive system mass leads to excessive weight and energy penalty. The differences could be ascribed to the use of a variable cruise altitude that is optimized depending on the chosen architecture and on the use of lower fidelity methods for the modelling of power modulation and distribution system components. Reference [33] does not show estimations for the more optimistic assumption so it is not possible to compare the latter results.

E. Optimized designs comparison

The star in Figure 12 indicates the starting point used for a localized optimization where the free control parameter of each architecture is used as design variable. To further optimize the resulting design with respect to the mission requirements, the PPU control parameters are not grouped together depending on the segment but are varied linearly for each mission segments. The resulting design vector therefore grows from two variables to twenty as starting and ending values are used for each of the ten segments considered (i.e. taxi, take-off, climb, cruise, descent, landing and diversion mission).

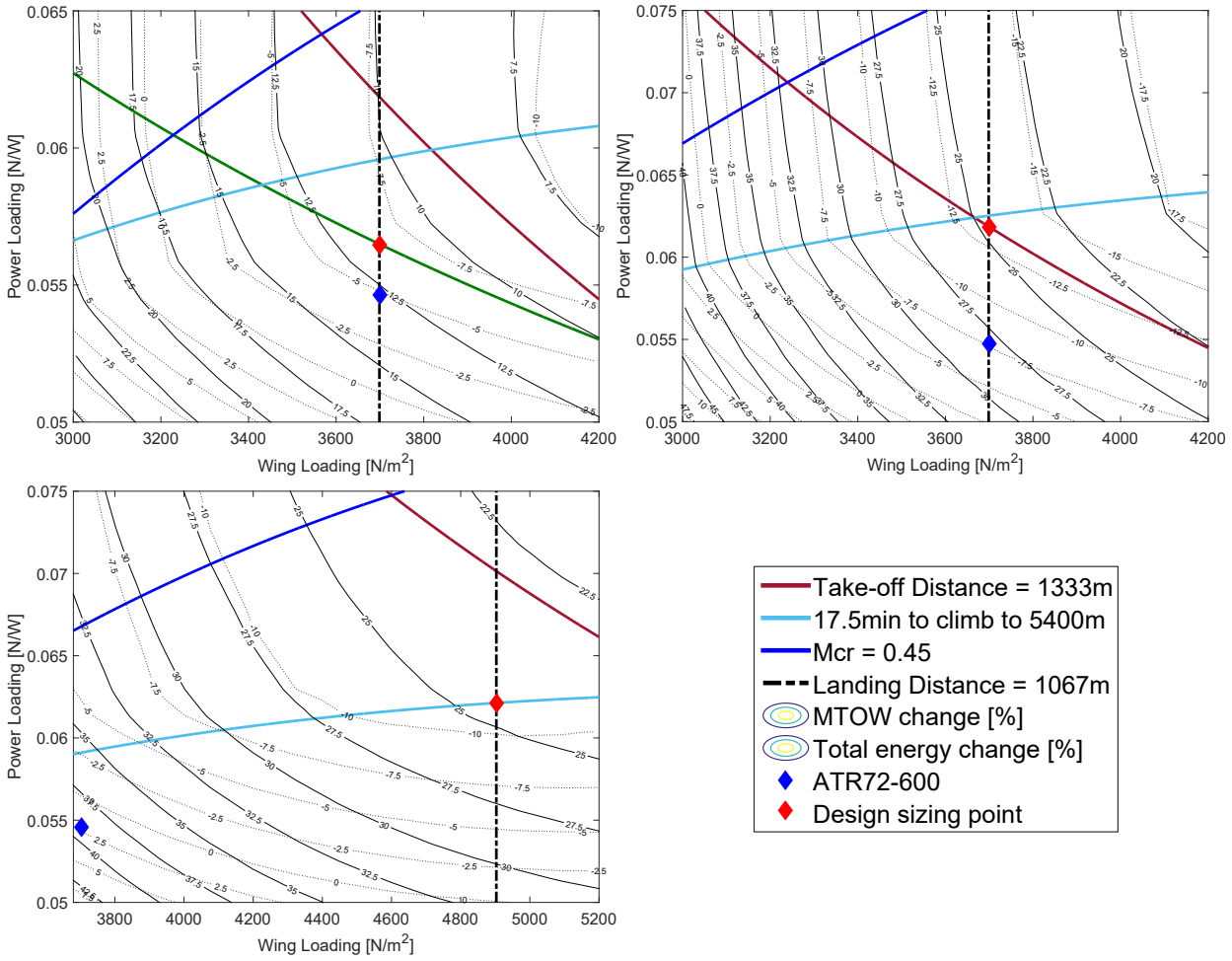

Fig. 13 Constraint diagrams with iso-mass (solid) and iso-energy (dashed) thumbprint plots. Upper right: parallel configuration. Upper left: series/parallel configuration. Lower right: DEP configuration.

Table 3 summarizes the results obtained from the local optimization routine with comparisons to the baseline design. The first two lines list the power-to-mass and wing-loading parameters derived from the constraint analysis. This analysis

uses the same constraints as the reference aircraft, namely FAR25/CS25 climb gradients, TOFL and LFL of 1333m and 1067 m respectively, a minimum ROC of 30 m/min at 3000 m and OEI conditions, a time to climb of 17.5 min to 5400 m and a cruise Mach number of 0.45.

The three constraint diagrams reported in Figure 13 show a zoomed-in image of design point for each of the three HEP architectures with the most constricting curves. Normally, the design point is chosen with a combination of the highest wing and power loadings so that for a given set of requirements, both the wing and propulsion system dimensions are minimized. As it can happen that these maxima do not coincide, iso-mass and iso-energy curves are overlain to show that for the studied designs the maximum wing-loading leads to better overall results.

Table 3 Summary and comparison with respect to the baseline design of the three HEP analysed. Optimistic maturity level assumption.

Configuration		**Baseline**	**Parallel**		**Hybrid**		**Series**	
Power to mass	kW/kg	0.176	0.174	-1%	0.168	-5%	0.158	**-10%**
Wing loading	kg/m^2	377	377	+0%	377	+0%	500	**+33%**
Wing								
Area	m^2	61.0	67.9	+11%	75.7	+24%	57.5	**-6%**
Span	m	27.0	28.6	+6%	30.1	+12%	26.3	**-3%**
Aerodynamics								
$C_{D,0}$	-	0.0307	0.0303	-1%	0.0293	**-4%**	0.0327	+7%
$C_{L,max}$	-	1.3	1.3	+0%	1.3	+0%	1.6	**+23%**
$C_{L,max,TO}$	-	2.2	2.2	+0%	2.2	+0%	3.1	**+41%**
$C_{L,max,L}$	-	3.2	3.2	+0%	3.2	+0.0%	4.2	**+33%**
Lift to drag ratio	-	16.9	17.2	+2%	18.8	**+11%**	17.4	+3%
Mass								
Max. take-off mass	t	23	25.6	**+11%**	28.5	+24%	28.8	+25%
Zero-fuel mass	t	21	21.8	**+4%**	22.4	+7%	22.4	+7%
Operative empty mass	t	13.5	14.3	**+6%**	14.9	+10%	15	+11%
Max. payload mass	t	7.5	7.5	+0%	7.5	+0%	7.5	+0%
Design fuel mass	t	2	1.7	-13%	1.4	**-29%**	1.5	-26%
Battery mass	t	0	2.1	NA	4.7	NA	4.8	NA
Propulsion								
PPU number	-	2	2	NA	6	NA	10	NA
Gas-turbine power	MW	4.1	3.1	-23%	2.6	-37%	0	**-100%**
Motor power	MW	0	1.3	NA	2.2	NA	4.5	NA
Generator power	MW	0	0	NA	0	NA	3.3	NA
Battery power	MW	0	1.7	NA	2.6	NA	3.2	NA
DoH_P	%	0	29.9	NA	46.6	NA	100	NA
$DoH_{P,\,Sources}$	%	0	34.5	NA	50.8	NA	49.4	NA
Energy								
Fuel energy	GJ	85.6	74.5	-12%	61.4	**-28%**	63.6	-26%
Battery energy	GJ	0	5.1	NA	12.3	NA	13.0	NA
Total energy	GJ	85.6	79.6	-7%	73.9	**-14%**	76.6	-11%
DoH_E	%	0	6.4	NA	17.0	NA	17.0	NA
Efficiency								
Avg. system efficiency	%	26.4	30.9	+17%	35.2	+33%	40.8	**+55%**
Avg. ESAR	m/MJ	19.1	20.4	+7%	22.2	+16%	25.7	**+35%**

The parallel architecture design shows a small improvement (around 1%) of the power-loading when compared to the baseline result. This is attributed to the fact that the boosted engine configuration suffers the same OEI penalty in case of PPU failure thus being limited by the second segment climb constraint as is the reference design. Moreover, no changes in terms of its wing-loading are considered as the external configuration is identical to the ATR72.

The second sub-figure illustrates that the parallel/series configuration could achieve a 9% higher power-loading when compared to the reference value. The wing-loading constraint is not affected by changes in drag coefficient or propulsive efficiency but only by the lift coefficient. For the second design it was assumed that the additional propellers would not have a large impact on the wing lift capabilities so the landing requirement in terms of wing-loading remains unchanged. On the other hand, the decrement of the induced drag allowed using tip mounted propellers positively influences the climb gradient requirement. The spreading of thrust over six PPUs also contributes in this improvement even when a higher gradient is used due to the larger number of propulsive devices (FAR25 and CS25 requirements change between 2 and 4+ engine configurations).

The third sub-figure show a 33% increase for the allowable wing-loading. This improvement is supported using lift-enhancing propellers along the entire span of the wing that characterizes the proposed DEP design. The higher lift-coefficient has also a positive impact on the take-off requirement. In addition, the OEI climb gradient constraint is greatly reduced in severity as the loss of one of the PPU equals to the loss of only 10% of the total propulsive power. All this results in making the time-to-climb requirement and landing constraint the sizing curves for this design allowing an improvement of the power-loading of around 11%. It is interesting to notice that the time-to-climb would most likely be a customer requirement and it could be relaxed to attain even larger benefits. This was not done in this study to ensure that all designs are sized with the same constraints and mission capabilities.

Table 3 summarizes the results for the baseline and the tree proposed designs. By observing the values in bold, it can be observed that each architecture excels in each area. The parallel design is the most similar to the baseline both in terms of external configuration and due to the low degree of hybridization. It is then the one that is least affected by the detrimental mass increase caused by the use of electric components on-board. However, the low DoH means also that this design sees the lowest benefits in terms of fuel and total energy reductions.

The series/parallel is characterized by the tip mounted propellers and the assumption that they would decrease the lift-induced drag. This translates into the highest lift-to-drag ratio among the design studied. The optimal control strategy for this design indicates that the electric motor should provide around half of the total propulsive power and they are thus used also during the cruise phase. The resulting battery and propulsive system mass greatly increase the aircraft MTOW but also lead to the largest reduction of fuel weight. The higher aerodynamic efficiency and overall system efficiency then ensure that the fuel reduction is translated also into a total energy saving of around 14%.

Finally, the DEP design is characterized by the best lifting capabilities. The increase of wing and power loadings are beneficial to the overall design as, even if it is the heaviest, it also has the smallest wing and comparable installed power to the parallel configuration. The large mass increase is due to the heavy battery derived by a high usage during cruise and by the very complex propulsive system. Considering this issue, the DEP design cannot achieve the same fuel and energy savings of the parallel/series configuration even though it is characterized by the highest improvement in terms of overall propulsive system efficiency.

IV. Conclusions

The presence of multiple energy sources and power paths characteristic of hybrid electric propulsive system architecture pose a challenge to well-established conceptual design procedure calling for the development of novel approaches. The method proposed in this study is based around the definition of a generic building block, the propulsive power unit, that can be combined into any of the most studied architectures configuration using few control parameters such as the number of units, the propulsive power share, the shaft power and the electric power ratios.

To fully capture the impact of changing propulsive system architecture, the effects needs to be integrated in all the steps characterizing the conceptual design process such as the constraint and mission analysis and the system mass estimation. With a design space exploration it was demonstrated that the control strategy of the electric system has a large influence on the overall results supporting the need for its integration at all level of the design process.

A low-fidelity approach was chosen for the sizing of the components by "rubberising" them so that they can be easily scaled to the required power rating. This process leads to fast design space exploration and improve the flexibility of the proposed approach at the cost of excluding secondary effects such as for example the worsening of specific power of electric motors as the cooling requirements are affected by the change of surface-to-volume ratio. The performance characteristics of these components are modelled with higher fidelity by assuming energy conversion

efficiency dependent on environment factors (altitude, speed, air temperature and density) and power requirements (e.g. current related losses in the cabling system, battery dynamic efficiency as function of its state of charge).

The method is first applied for an extensive design space exploration where the effects of propulsive system architecture, control strategy and technology maturity of the components have been assessed. For the more conservative estimations, the parallel and parallel/series design show little to no improvements in terms of fuel and total energy consumption with possible savings of around 5% even for the best combination of settings. The distributed series configuration sees a large increase of both maximum take-off mass and energy consumption with a minimum of +30% clearly indicating that this configuration is not suitable unless a leap in performance is seen for the electric machines and battery's technology.

When looking at the more optimistic assumption we can see that the electrification of the propulsion system becomes more interesting. The low hybridization of the parallel architecture limits its benefits in terms of fuel and energy reductions to around 12% and 7% respectively. The series design sees the largest change to its performances thanks to the high system efficiency and to a less punishing battery induced mass increase leading to possible savings in the range of 26% for fuel and 11% for energy requirements. Finally, the combination of an improved aerodynamic and propulsive system efficiency results in the parallel/series being the best configuration for the reduction of fuel and energy consumption by about 28% and 14% with respect to the baseline design.

Focusing on the causes for these improvements, it is found that the electrification of the propulsive system and its use to improve the aerodynamic performances can lead to beneficial changes in terms of wing and power loadings. For the parallel architecture no significant changes are observed as the interaction between the propulsive units and the rest of the aircraft system is not substantially different from the conventional baseline case. On the other hand, the use of tip mounted propellers in the series/parallel configuration has the twofold effect of reducing the lift-induced drag and spreading the thrust requirement over a larger number of propulsive devices greatly relaxing the constricting requirements leading to a 5% increase of its power-loading. The distributed propulsion design sees also a 10% improvement thanks to its increased lift capabilities that allow the use of a 33% higher wing-loading without scarifying the aircraft field capabilities.

Overall, it is concluded that the choice of hybrid electric propulsive system architecture is dependent on the performance capability attained by the electric components, in particular of the battery. If a large leap in their technology is achieved, any configuration that couples a high degree of hybridization with the opportunity to improve the aircraft aero-propulsive characteristics will lead to large savings in terms of fuel consumption. However, if the battery and motor technology does not advance significantly from the more conservative estimations, the use of hybrid propulsive design is questionable and only simpler configurations characterized by low degree of hybridization will make economic sense.

References

[1] Ashcraft, S. W., Padron, A. S., and Pascioni, K. A., "Review of Propulsion Technologies for N+3 Subsonic Vehicle Concepts," Tech. Rep. October, Glenn Research Center, NASA, Cleveland, Ohio, 2011. doi:NASA/TM-2011-217239.

[2] Pornet, C., and Isikveren, A. T., "Conceptual design of hybrid-electric transport aircraft," *Progress in Aerospace Sciences*, Vol. 79, 2015, pp. 114–135. doi:10.1016/j.paerosci.2015.09.002.

[3] Hepperle, M., "Electric Flight–Potential and Limitations," Tech. rep., German Aerospace Center, Braunschweig, 2012.

[4] Thole, K. A., Whitlow, W., Benzakein, M. J., and Csonka, S. J., *Commercial Aircraft Propulsion and Energy Systems Research: Reducing Global Carbon Emissions*, 2016. doi:10.17226/23490.

[5] Madavan, N. K., Del Rosario, R., and Jankovsky, A. L., "Hybrid-Electric and Distributed Propulsion Technologies for Large Commercial Air Transports : A NASA Perspective " Advanced Air Transport Technology Project "," , 2015.

[6] Nam, T., Soban, D., and Mavris, D., "Power Based Sizing Method for Aircraft Consuming Unconventional Energy," *43rd AIAA Aerospace Sciences Meeting and Exhibit*, , No. January, 2005, pp. 1–13. doi:10.2514/6.2005-818.

[7] Pornet, C., Gologan, C., Vratny, P. C., Seitz, A., Schmitz, O., Isikveren, A. T., and Hornung, M., "Methodology for Sizing and Performance Assessment of Hybrid Energy Aircraft," *Journal of Aircraft*, Vol. 52, No. 1, 2015, pp. 341–352. doi:10.2514/1.C032716.

[8] Schneegans, A., "Investigating Systems Architectures At the Aircraft Level – Towards a Holistic Framework for the Aircraft Systems Design Process," Tech. rep., PACE Aerospace Engineering and Information Technology GmbH, 2010.

[9] Roskam, J., *Airplane Design*, DARcorporation, 1985.

[10] Zamboni, J., "A method for the conceptual design of hybrid electric aircraft," , 2018. URL https://repository.tudelft.nl/islandora/object/uuid:7b7dc56b-6647-4cc9-98f6-2ed5d488c759?collection=education.

[11] Hoogreef, M. F. M., Vos, R., De Vries, R., and Veldhuis, L. L. M., "Conceptual Assessment of Hybrid Electric Aircraft with Distributed Propulsion and Boosted Turbofans," *Proceedings of the 2019 AIAA Aerospace Sciences Meeting*, American Institute of Aeronautics and Astronautics, San Diego, CA, USA, 2019.

[12] Raymer, D. P., *Aircraft design: A conceptual approach*, AIAA Education Series, 2012. doi:http://dx.doi.org/10.2514/4.869112.

[13] Borer, N. K., Patterson, M. D., Viken, J. K., Moore, M. D., Bevirt, J., Stoll, A. M., and Gibson, A. R., "Design and Performance of the NASA SCEPTOR Distributed Electric Propulsion Flight Demonstrator," *16th AIAA Aviation Technology, Integration, and Operations Conference*, 2016. doi:10.2514/6.2016-3920.

[14] Stoll, A. M., and Veble Mikic, G., "Design Studies of Thin-Haul Commuter Aircraft with Distributed Electric Propulsion," *16th AIAA Aviation Technology, Integration, and Operations Conference*, 2016. doi:10.2514/6.2016-3765, URL http://arc.aiaa.org/doi/10.2514/6.2016-3765.

[15] Mirande, L., and Brennan, J., "Aerodynamic effects of wingtip-mounted propellers and turbines," *4th Applied Aerodynamics Conference*, 1986. doi:10.2514/6.1986-1802.

[16] Thauvin, J., Barraud, G., Budinger, M., Roboam, X., Leray, D., and Sareni, B., "Hybrid Regional Aircraft: A Comparative Review of New Potentials Enabled by Electric Power," *52nd AIAA/SAE/ASEE Joint Propulsion Conference*, 2016. doi:10.2514/6.2016-4612.

[17] Seitz, A., Isikveren, A. T., and Hornung, M., "Pre-Concept Performance Investigation of Electrically Powered Aero-Propulsion Systems," *49th AIAA/ASME/SAE/ASEE Joint Propulsion Conference*, 2013, pp. 1–16. doi:10.2514/6.2013-3608.

[18] Ruijgrok, G. J. J., *Elements of airplane performance*, Delft University Press, 2009.

[19] Lorenz, L., Seitz, A., Kuhn, H., and Sizmann, A., "Hybrid Power Trains for Future Mobility," *Deutscher Luft- und Raumfahrtkongress*, 2013, pp. 1–17.

[20] Torenbeek, E., *Synthesis of subsonic airplane design*, Delft University Press, Delft, 1979. doi:10.1007/978-94-009-9580-2, URL https://repository.tudelft.nl/islandora/object/uuid{%}3A229f2817-9be9-49b6-959a-d653b5bac054http://link.springer.com/10.1007/978-94-009-9580-2.

[21] Stückl, S., "Methods for the Design and Evaluation of Future Aircraft Concepts Utilizing Electric Propulsion Systems," Phd dissertation, Munich Technical University, 2016.

[22] Hoelzen, J., Liu, Y., Bensmann, B., Winnefeld, C., Elham, A., Friedrichs, J., and Hanke-Rauschenbach, R., "Conceptual design of operation strategies for hybrid electric aircraft," *Energies*, Vol. 11, No. 1, 2018, pp. 1–26. doi:10.3390/en11010217.

[23] Strack, M., Pinho Chiozzotto, G., Iwanizki, M., Plohr, M., and Kuhn, M., "Conceptual Design Assessment of Advanced Hybrid Electric Turboprop Aircraft Configurations," *17th AIAA Aviation Technology, Integration, and Operations Conference*, 2017. doi:10.2514/6.2017-3068, URL http://arc.aiaa.orghttps://arc.aiaa.org/doi/10.2514/6.2017-3068.

[24] Gerssen-Gondelach, S. J., and Faaij, A. P. C., "Performance of batteries for electric vehicles on short and longer term," *Journal of Power Sources*, Vol. 212, 2012, pp. 111–129. doi:10.1016/j.jpowsour.2012.03.085.

[25] Thackeray, M. M., Wolverton, C., and Isaacs, E. D., "Electrical energy storage for transportation—approaching the limits of, and going beyond, lithium-ion batteries," *Energy & Environmental Science*, Vol. 5, No. 7, 2012, pp. 7854–7863. doi:10.1039/c2ee21892e.

[26] Antcliff, K. R., and Capristan, F. M., "Conceptual Design of the Parallel Electric-Gas Architecture with Synergistic Utilization Scheme (PEGASUS) Concept," *18th AIAA/ISSMO Multidisciplinary Analysis and Optimization Con*, 2017. doi:10.2514/6.2017-4001, URL http://arc.aiaa.org.

[27] Snyder, Jr., M. H., and Zumwalt, G. W., "Effects of wingtip-mounted propellers on wing lift and induced drag." *Journal of Aircraft*, Vol. 6, No. 5, 1969, pp. 392–397. doi:10.2514/3.44076, URL http://arc.aiaa.org/doi/10.2514/3.44076.

[28] Patterson, J. C., and Bartlett, G. R., "Evaluation of installed performance of a wing-tip-mounted pusher turboprop on a semispan wing," *NASA Technical paper*, , No. August, 1987. URL https://www.tib.eu/en/search/id/ntrs{%}3Asid{~}oai{%}253Acasi.ntrs.nasa.gov{%}253A19870016608/Evaluation-of-installed-performance-of-a-wing-tip/?tx{_}tibsearch{_}search{%}5Bsearchspace{%}5D=tn.

[29] Stoll, A. M., Bevirt, J., Moore, M. D., Fredericks, W. J., and Borer, N. K., "Drag Reduction Through Distributed Electric Propulsion," *14th AIAA Aviation Technology, Integration, and Operations Conference*, 2014, pp. 16–20. doi:10.2514/6.2014-2851, URL http://www.jobyaviation.com/LEAPTech(AIAA).pdfhttp://arc.aiaa.org/doi/10.2514/6.2014-2851.

[30] Hepperle, M., "Aspects of Distributed Propulsion - A View on Regional Aircraft," , 2016. URL https://www.mh-aerotools.de/company/paper{_}16/Hepperle-ElektrischesFliegenStuttgart2016.pdf.

[31] Felder, J., Kim, H., and Brown, G., "Turboelectric Distributed Propulsion Engine Cycle Analysis for Hybrid-Wing-Body Aircraft," *47th AIAA Aerospace Sciences Meeting including The New Horizons Forum and Aerospace Exposition*, 2009, pp. AIAA 2009–1132. doi:10.2514/6.2009-1132.

[32] Seitz, A., Schmitz, O., Isikveren, A. T., and Hornung, M., "Electrically Powered Propulsion: Comparison and Contrast to Gas Turbines," *Deutscher Luft- und Raumfahrtkongress 2012*, 2012, pp. 1–14. doi:281358.

[33] de Vries, R., Hoogreef, M. F. M., and Vos, R., "Preliminary Sizing of a Hybrid-Electric Passenger Aircraft Featuring Over-the-Wing Distributed-Propulsion," *Proceedings of the 2019 AIAA Aerospace Sciences Meeting*, American Institute of Aeronautics and Astronautics, San Diego, CA, USA, 2019.